1 Introduction

Every year large quantities of mineral aerosol are injected into the atmosphere. Mineral dust accounts for approximately 75% of the global aerosol mass load and 25% of the global aerosol optical depth (Kinne et al., 2006). It is mainly released to the atmosphere, especially from the Sahara and nearby deserts (Christopher et al., 2013, 2015; Schepanski et al., 2016; Francis et al., 2017).

Dust affects strongly the Earth's radiation budget (Mahowald et al., 2006; Balkanski et al., 2007; Otto et al., 2009; Bierwirth et al., 2009; Müller et al., 2011; Yoshioka et al., 2007; Papadimas et al., 2012; IPCC, 2013). Dust particles modify microphysical cloud properties, acting as condensation and ice nuclei (Balis et al., 2002; Zerefos et al., 2002; Sassen et al., 2003). The effects of mineral dust on human health and ecosystems (Sultan et al., 2005; Pérez et al., 2008; Polymenakou et al., 2008; Tobıas et al., 2011a.b; Stafoggia, et al., 2016; Middleton, 2017) through the transport of micro-organisms are notable (Kallos et al., 2006; Escudero et al., 2005, 2007; Mitsakou et al., 2008; Morman and Plumlee, 2013). Strong dust events affect air and road transport, reducing the visibility (e.g., Pauley et al., 1995; Lorenz and Myers, 2005).

Most of the African dust particles are transported westwards over the Atlantic (Viana et al., 2002; Alastuey et al., 2005; Schepanski et al., 2009a). However, a considerable part of dust is also transported northerly, affecting the southern European region (Papayannis et al., 2005; Escudero et al., 2005; Balis et al., 2006; Pérez et al., 2006.b; Kallos et al., 2006; Kocak et al., 2007; Gerasopoulos et al., 2006; Papadimas et al., 2008; Lyamani et al., 2006b; Guerrero-Rascado et al., 2008; Mitsakou et al., 2008; Basart et al., 2009; Pavese et al., 2009; Gkikas et al., 2009; Guarnieri et al., 2011; Valenzuela et al., 2012; Nava et al., 2012; Marconi et al., 2014; Mandija et al,. 2017, Cachorro et al, 2016), more northerly (Ansman et al., 2003; Coen et al., 2004; Vukmirovic et al., 2004; Klein et al., 2010), and even as far as Britain and Scandinavia (Franzen et al., 1994 ; Ryall et al., 2002). Saharan dust is generally transported over the Mediterranean basin by cyclone winds (Moulin et al., 1998; Escudero et al., 2005; Kallos et al., 2006; Querol et al., 2009a; Schepanski et al., 2009b, 2011; Fiedler et al., 2014; Flaounas et al., 2015). Sharav cyclones facilitate dust mobilization over North Africa deserts enabling their transportation over the Mediterranean basin. Frequent dust events are observed especially in the Mediterranean region (Toledano et al., 2007; Papayannis et al., 2008, 2009; Pey et al., 2013; Schepanski et al., 2016; Sicard et al., 2016; Mandija et al,. 2016; Gkikas et al., 2016).

Aerosol optical and microphysical properties during dust events are intensively investigated using several methodologies; like active and passive remote sensing techniques from AERONET and EARLINET networks (Hamonou et al., 1999; Gobbi et al., 2000; Holben et al., 2001; Bosenberg et al., 2001; di Sarra et al., 2001; Gobbi et al., 2002; Carnuth et al., 2002; Müller et al., 2003; Ansmann et al., 2003; Dulac and Chazette, 2003; Gobbi et al., 2004; Papayannis et al., 2005; Mona et al., 2006; Sicard et al., 2006, 2011; Lyamani et al., 2005, 2006.a; Papayannis et al., 2008; Liu et al., 2008; Alados-Arboledas et al., 2008; Guerrero-Rascado et al., 2009; Navas-Guzman et al., 2013; Pappalardo et al., 2014), satellite data from MODIS, TOMS, etc. (Israelevich et al., 2002; Barnaba and Gobbi, 2004; Jamet et al., 2004; Marinou et al., 2016) and model products like BSC-DREAM, NAAPS, SIKRON, etc. (Christensen, 1997; Nickovic et al., 2001; Draxler and Rolph, 2003; Papayannis et al., 2008).

This work is a more generalized study on desert dust intrusions over Europe compared to the previous studies, in the sense that the analysis considers the whole continental area and not only its southern part or sporadic events in the northern part of the continent. In addition to these large-scale analyses, the validation of model products using sunphotometer and satellite-based measurements are provided. The main goal of this work is to determine the climatology of the dust intrusions over the European continent for a 9-year time-period, 2006-2014, based on data from the BSC- DREAM8b_v2.0 model. The use of model products and of BSC-DREAM was required since this model is a tool able to provide a full coverage of aerosol properties over the entire European continent and the principal dust sources. Models are also an appropriate tool for the climatology over large domains and long periods of time. Moreover, satellite products are an additional tool for aerosol investigation over large domains. Satellite-based products are used to estimate the model uncertainties. The aerosol optical depth (AOD) was chosen for the analysis because it can be easily and extensively compared to AOD measurements. Further analyses are done to find the principal sources affecting the continent and to determine their contribution to several European regions. Statistical estimation of the variability of mean AOD and the number of dust events over distinct sectors is carried out. In addition, main scenarios of dust intrusions over the central and northern European regions and the differences between western, central and eastern dust events are investigated. The climatology of dust emissions over the desert regions and their relationship with dust intrusions over Europe is analysed. Finally, a case study of dust intrusion is further investigated with the support of ground- and satellite-based remote sensing measurements and back-trajectory models.

2 Methodology

This investigation is carried out using the data taken from the model BSC-DREAM8b_v2.0 the Atmospheric Dust Forecast System, http://www.bsc.es/ESS/mineral_dust_database (Nikovic at al., 2001; Pérez et al., 2006.a; Todd et al., 2008; Basart et al., 2012). This model supplies AOD550_DUST and EMI_DUST (dust emission rate) data from 1 January 2006 up to 31 December 2014. From 2006, the model was upgraded to cover the northern Europe, southern Sahara, and Arabian Peninsula. AOD is a fundamental parameter measured by sunphotometers as those operating in AERONET (Holben et al., 1998). The spatial coverage of this model includes the major part of the European continent (except its northern part) and the sectors of the two deserts under investigation Sahara and Arabia (Latitude [0^{o} – 65^{o}N]; Longitude [25^{o}W – 60^{o}E]). The BSC-DREAM outputs have been validated and tested in several studies, and have shown good agreement with AERONET data and satellite observations or field campaigns (SAMUN) in a number of studies (Ansmann et al., 2003, Papayannis et al., 2005; Balis et al., 2006; Pérez et al., 2006a;b; Jiménez-Guerrero et al., 2008; Haustein et al., 2009; Pay et al., 2010, 2012; Basart et al., 2012). Nevertheless, the model underestimates AOD in regions where dust is contaminated with fine mode particles (Pérez et al., 2006b). Dust load is underestimated in the Sahel in spring and overestimates it in the Middle East in the summer as well as in Northern Algeria (Basart et al., 2012). More detailed information about the model performance and associated uncertainness can be found in the intercomparison studies (Basart et al., 2012; Huneeus et al. 2016; Todd et al. 2008).

In addition, the transport model HYSPLIT4 (Hybrid Single Particle Lagrangian Integrated Trajectory Model, http://ready.arl.noaa.gov/HYSPLIT.php) is used to identify patterns of back-trajectories originating over the desert areas. Among the various outputs of this model, here we have used the clusters of the principal dust sources and the footpaths of the trajectories of air masses at various altitudes (usually 1000 - 6000 m).

The study is split into two main steps; the analysis of the dust event climatology over the European continent, and then, an investigation of the influence of the desert sectors over European sectors, using BSC-DREAM data of the optical depth of dust particles (AOD550_DUST), aerosol optical depth over the plume area (AOD_p), dust emission rate (EMI_DUST), and HYSPLIT trajectories to identify the potential dust sources. AOD_p is calculated as the mean value of the AOD500_DUST over areas where this parameter is higher than 0.1, and hence it measures mean AOD over the dust plumes. To investigate the dust event climatology, we have divided the affected area (European continent) and desert area (Saharan and Arabian Deserts) into several sectors (Fig. 1). In terms of spatial coverage, the European area is divided into twelve sectors (I - XII), with latitudes (37^o; 44^o; 51^o; 58^o) and longitudes (-10^o; 5^o; 20^o; 35^o; 50^o). The same longitudes are used as well to define the four desert sectors (XIII - XVI), with latitudes (14^o - 34^o). A 9-year model simulation was performed at 0.33ºx0.33º spatial resolution and 1-hr temporal resolution. The model operated in all days, where AOD and EMI data were available during this period. The model outputs are publicly available on the website of the Barcelona Supercomputing Center, in NetCDF format.

Determination of the most exposed areas of the European continent is done using the daily and monthly-averaged AOD550_DUST provided by BSC-DREAM. The model forecasts dust plumes based on the AOD level. A dusty day in a certain sector is considered a day in which are observed areas with mean AOD_p>0.1. These areas are called dust plumes. The minimal area of a dust plume, based on the model spatial resolution, is about 720 km^2. This threshold is chosen in accordance with the thresholds for dust event identification used in previous studies (Toledano et al., 2007; Nabat et al., 2009; Papayannis et al., 2008; Kaskaoutis et al., 2012; Kumar et al, 2014; Gkikas et al., 2012, 2013; 2016). In any case, the sectoral average AOD_{550} may be lower during dusty days, because it deals with the average value over wider domains.

The model evaluation includes ground-based and satellite-based measurements. BSC-DREAM8b v2.0 model outputs are compared against the direct observations from AERONET and MODIS. There are compared the hourly point data of AOD550_DUST provided by the model to the coarse mode contribution on AOD_{550} provided by the model to AERONET at selected stations, during the respective hours. AERONET data level 2.0 are used. When data of level 2.0 aren't available, data of level 1.5 are used. These data are taken only during sunny hours. AERONET AOD has low uncertainty (0.01–0.02), and high temporal resolution (15 min) (Eck et al., 1999). This dataset can be viewed as the "ground truth" for the substantiation of the model outputs. The accuracy of MODIS AOD is significantly worse than AERONET AOD especially over land and coastal regions. MODIS AOD has an expected error of ±(0.05+0.15AODaeronet) over land and ±(0.03+0.05AODaeronet) over the ocean (Kahn et al., 2011). The AERONET products are used for globally satellite validation too. Here, the satellite data (MYD04_L2) are provided by MODIS (Aqua) Deep Blue Aerosol Optical Depth (Land), collection 6.1. The sensor/algorithm resolution is 10 km at nadir, imagery resolution is 2 km at nadir, and the temporal resolution is daily. In general, MODIS provides AOD data comparable to AERONET, characterized by high correlation, 0.86 (Levy et al., 2013).

3 Results and discussions

3.1 Distribution of AOD_{550} over the European sectors

The distribution of the principal characteristics of dust events over each European sector are presented in this section. Table 1 presents the distribution of the data of AOD_p, NDD and PA. AOD_p is the average AOD_{550}, only over the areas covered by the dust plume (areas where $AOD_{550}>0.1$). Number of days (NDD) where dust plumes are present ($AODp>0.1$) over twelve European sectors are represented in this table.

The total number of dusty days at every European sector, presented in the table 1 was 6885, where 81% of them occur in southern sectors, 16.6% in the central sectors and only 2.4% in the northern sectors. However, these numbers represent dust events in each sector, even though the same event can cover more than one-sector simultaneously. This is an appropriate number to analyse the climatology of these events at each sector, but overestimates the number of dust events over the whole continent.

Dust events occur in 33-49% of the annual days at the southern sectors, 6-11% at the central sectors and less than 2% at the northern sectors. Comparable results are obtained by Pey et al. (2013), who reported that the Mediterranean sectors are affected by the African dust outbreaks at 30-37% of annual days.

The southern sectors are characterized by the highest values of AOD_p. Mean AOD_p over the sectors I-IV is 0.155. Gradual decrease of the mean AOD_p toward the northern sectors is observed. The mean AOD_p in the central and northern sectors are 0.132 and 0.122, respectively.

Mean percentage area (PA) is used to show the fraction of each sector area covered by the dust plume ($AOD_p>0.1$). Mean PA in the southern sectors was 13-20%, while in central and in the northern sectors were almost the same 10-17% and 9-18% respectively. Mean PA values have moderate correlation with AOD_p. The correlation coefficients (CC) between hourly data of PA and AOD_p ranges between 0.55 (sector XII) and 0.79 (sector VIII), with mean value 0.69. The highest PA obtained in the southern, central and northern sectors, coincide with the maximum AOD_p. Some differences are found in the case of the NDD, whose maximums don't correspond completely to those of PA.

The sector II has the highest mean value of the plume AOD_p (0.18). Moreover, high number of dusty days (1615) and PA (24%) are observed in this sector. These facts indicate this sector is the most affected European sector by dust intrusions. Furthermore, the western sector I has the second highest AOD_p (0.16). The other sectors have lower AOD_p (0.12-0.14). However, the difference between the mean values of AOD_p is not significant. The fact that the mean values of AOD_p have weak dependence on the sectors is related to the determination of the AOD_p as the average AOD in the dust plumes. This parameter shows how intense are the dust plumes, but it is not directly related to the dust events over each sector, which is represented better by the number of dusty days. Indeed, NDD show a significant variation over different sectors.

Hourly data of AOD550_DUST over the whole continent, downloaded from the BSC-DREAM website, are used to define the seasonal variations of the mean AOD over the region. Fig. 2 presents these maps for four seasons; June-July-August (JJA) and September-October-November (SON), December-January-February (DJF), March-April-May (MAM). A first look at the four plots of the fig. 2 proposes that the mean AOD550_DUST affect more the southern sectors, especially the Italic peninsula (highest mean AOD). Meanwhile, the northern sectors are less

affected, especially the United Kingdom (lowest mean AOD). The variations of the mean AOD550_DUST at both sectors show a similar tendency: higher during summer and lower during winter. These variations are more evident in the highly affected sectors. Mean AOD550_DUST in the summer was 0.01 at the center of the European continent, reaching up to 0.1 at the southern Mediterranean Sea, while it reached extreme values in the central Sahara and the Arabian Peninsula (0.7). The second highest seasonal mean AOD_{550} is found during spring over the European continent. Meanwhile, winter seasons present the lowest mean AOD in Europe (up to 0.01) and nearby deserts (up to 0.10).

3.1.1 Latitude-gradients of the desert dust characteristics

The mean number of the dusty days in the southern, central and northern sectors, were 1395, 286 and 41, respectively. Higher NDD are noted in the southern sectors. The result that indicates that the most affected sectors are in the south of the continent was expected, because of their vicinity to the Saharan Desert. Previous studies (Barnaba and Gobbi, 2004; Pey et al., 2013) show that AOD and PM_{10} decrease exponentially with the latitude. From this viewpoint, only 20.5% of the dust events in southern sectors progress toward the central sectors, and only 14.3% of them progress further toward the northern sectors. Even though strong latitude-gradients of NDD are observed. The mean of the AOD_p over the areas covered by dust plumes and the PA, demonstrate slight gradients. Respectively, 0.155±0.058, 0.135±0.038 and 0.124±0.024 are the mean AOD_p values of dust plumes, in the southern, central and northern areas (AOD_{550}>0.1). Meanwhile, respective mean PA are 18.0±21.3, 13.1±16.1 and 12.6±15.9. The South, Central and North in fig. 3, are defined as the middle latitudes of the southern (40.5^{o}N), central (47.5^{o}N) and northern (54.5^{o}N) European sectors.

The gradients of the NDD from southern to central and from central to northern sectors was relatively high, 79-86% respectively. However, AOD_p and AP present much lower gradients, 13-8% and 26-3%. An interesting result, is that eastern central sectors have the lowest gradient of the AOD_p (8%), but the strongest gradients of the AP (31%). This is due to the low gradient of AOD_p between the sectors IV and VII, and high gradient of AP between the sectors VII and XI. Surprisingly, an increment of 43% of the AP from the sector VI to the sector X was observed.

Low precipitation rates in the south of Europe favor the relatively long residence time of desert dust particles in the atmosphere. The probability that a dust plume to encounter rain increases toward the north of the European continent. This fact and the lower dust intrusions over the northern sectors, explain the sharp gradients in AOD_{550} in the south-north direction.

3.1.2 Longitude-gradients of the desert dust characteristics

Other important results obtained are the longitude-gradients of above-mentioned dust event characteristics. AOD_p, NDD and AP depend on the longitude, for both, the southern, central and northern sectors (Fig. 4). The West, Central and East in fig. 4 are defined as the middle longitudes of the sectors I, II, III and IV; 3.5^{o}W, 12.5^{o}E, 27.5^{o}E and 42.5^{o}E.

NDD at the southern sectors show an irregular variation without any tendency, same as in the case of the sectoral mean AOD_{550}. NDD at the central and northern sectors has a slight maximum at mid-longitude sectors and

decreasing gradually toward to the east and west. Quite similar variations of AOD_p are observed at both, southern, central and northern sectors. A slight increase from the western to central sectors, and then a gradual decrease toward the eastern sectors is evidenced. More irregular variations are observed in the case of PA. Central sectors have the maximal AP, while the western and eastern sectors have the minimal AP. In short, the central and especially the central-east sectors have the maximal NDD, AOD_p and AP, especially in the southern region.

Dust intrusions over the central sectors are more likely to reach northern sectors than those over-passing western and eastern sectors. Highest AOD_p and the number of dust events in the central sectors support this statement. 23-32% of their dust events penetrate in central sectors and 3-5% in the northern sectors. Meanwhile, in the western and eastern sectors, only 14% of dusty days penetrate in central sectors and only 2-3% in the northern sectors. The highest number of dust events in the southeastern sector IV was not reflected in the sector VIII. This is due to the lower intensity of the northward winds or the northwestward winds, which transport the dust from sector IV to the sector VII and VIII.

In previous studies, Querol et al. (2009.a, b) reported an increment of aerosol load toward the eastern Mediterranean regions. Barnaba and Gobbi (2004) reported a seasonal dependence of longitudinal gradients of the AOD, results which are in good accordance with the findings in the section 3.3.2. Highest AOD at the mid-longitude sectors is reported also by Pey et al. (2013).

3.2 Statistical distributions of BSC-DREAM data

An important parameter, which indicates how intensive the dust events are, is the frequency distribution of the AOD_p data. Northern sectors are expected to show a distribution limited to lowest AOD, but the southern distributions are expected to be more extended to the higher AOD values. The frequency distributions (%) of all mean data of AOD_p for all sectors are presented in the table 2. The values are calculated as percentages of the number of days with mean AOD_p at each bin to the total number of dusty days.

The mean AOD_p is low, especially at the mid-latitude and northern European sectors. In this contest, most of dust events in all sectors is characterized by the lowest AOD_p (0.1-0.2). Even almost similar, the statistical distributions present some singularities. Southern sectors (especially sector II) have the lowest fractions of the $AOD_p<0.2$ data, 74-94%, while this percentage of central sectors were significantly higher, 90-97%. Meanwhile, in only one northern sector (sector X) AOD_p was found higher than 0.2. In the southern sectors, AOD data are more distributed at higher AOD values, due to the vicinity of these sectors to desert areas. AOD_p data at intervals (0.2-0.3) present 5-19% at southern sectors and 3-8% at central sectors. In addition, 7.5% of the AOD_p data on the northern sector X are higher than 0.2. Despite the significant latitude-decay of the percentile $AOD_p>0.2$ data, a strong longitude variation was observed. The sector I and especially sector II, and their northern neighbor sectors (V, VI, and X) show the highest percentile of $AOD_p>0.2$ data. In southern sectors I and II, there are found also AOD_p data higher than 0.5, while only in one central sector (sector VI), there is obtained AOD_p higher than 0.4. Table 3 presents the statistical distribution of the PA data. Dust plume sectoral coverages of 10% (PA10) are observed in 41-61% of cases at the southern sectors, 51-69% and 45-72% at the central and northern sectors respectively. The mean PA10 at all sectors is 59%, while PA20 and PA30 are 17% and 9%, respectively. In 16% of all the cases there are obtained PM1.

Moreover, in only 2% of all cases, dust plumes cover only 0.1% of the sector area, which is about approximately the area of the spatial resolution of the model. In short, two southwest sectors, I and II, are the most affected sectors by the intense dust intrusions, having the highest fractions of the high AOD_p.

3.3 Climatology of AOD at the European sectors; annual and inter-annual variability

3.3.1 Annual cycles of AOD at the European sectors

Annual cycles of the aerosol optical depth inside of the dust plumes (AOD_p) and the percentage areas covered by these plumes, at southern and central European sectors are shown in fig. 5. Mean values of AOD_p are obtained by averaging AOD_p data for all sectors at each month. This figure presents the mean annual cycles of the AOD_p over eight European sectors. These cycles are retrieved by averaging AOD_p data provided by BSC-DREAM over the period 1 January 2006 – 31 December 2014. There are used monthly means of the daily mean AOD_p data in all the investigated sectors.

The annual cycles indicate that mean AOD_p values in the southern sectors reach their peak during the period April - June (western sectors I and II) and during March-May (eastern sectors III and IV). However, this pattern is not the same in all sectors. The peaks for each sector are found as follows; sector I (0.20) in May, sector II (0.21) in June, sector III (0.17) in April and sector IV (0.16) in March. So, the maxima on the southeastern sectors are obtained in spring, while in the southwestern sectors the maxima are found postponed to the late spring-early summer. Previous results for the sector I (Moulin et al.., 1998; Alados-Arboledas et al., 2003; Toledano et al., 2007; Mateo et al., 2015; Cachorro et al., 2016), suggested that the Iberian Peninsula is affected by dust events during the summer seasons, Italic Peninsula (sector II) during the spring and summer seasons (Moulin et al., 1998; Barnaba and Gobi, 2004; Basart et al., 2009; Gkikas et al., 2013), while the southeastern sector (sector III) during the spring seasons (Moulin et al.., 1998; Barnaba and Gobi, 2004; Basart et al., 2009; Kaskaoutis et al., 2012; Gkikas et al., 2013). The shape of the AOD_p annual cycle of sector I is like the one of Mallorca, a background site in the western Mediterranean basin, established by Sicard et al. (2016) from AERONET measurements. However, the peaks are displaced one month (July in Sicard et al., 2016; June in this study) because of the influence of pollution events which trigger in July taken into consideration in Sicard et al. (2016) and not here.

Almost similar patterns of annual cycles are found in the AOD_p data over the four central sectors, reaching their maxima (0.13-0.16) during the period April – June. The maxima at the sectors V and VII are obtained in May (respectively 0.15 and 0.14), while the maxima at the sector VI (0.16) is obtained in June. Meanwhile, the maxima of the eastern sector VIII (0.13) is obtained earlier, in April. Because of scarce dust intrusions over the northern sectors, no regular annual cycles can be retrieved for the AOD_p.

Annual cycles of AOD_p at the desert sectors have different peculiarities. First, the eastern Sahara region (sector XV) has the lowest maxima (0.24). The AOD_p maxima at the three other sectors is almost the same (0.38-0.42). The sectors XIII and XVI reach their AOD_p maxima during summer, June-July. Meanwhile, the two other sectors XIV and XV, reach their maxima earlier, during the period April-June. These results are in good agreement with previous studies about Saharan dust intrusions over certain regions of Europe (Moulin et al., 1998; Papayannis et al., 2005; Barkan et al., 2005; Mona et al., 2006; Papayannis et al., 2008).

Annual cycles of the percentage area (PA) follow almost the same patterns of the cycles of AOD_p. The mean value of the correlation coefficients (CC) between monthly mean values of the AOD_p and PA is relatively high, 0.84±0.06. Both southern-western sectors I and II reach their maxima of PA during the late spring and summer period. On the other side, the two southern-eastern sectors III and IV reach their PA maxima earlier, during late spring and early summer (March-June). However, the central sectors don't show regular annual PA cycles.

Almost the same annual cycles are found also with the monthly mean of NDD. NDD days at the southern sectors are more distributed over the entire year. This fact is reflected by the percentage data of NDD during each month, which at southern sectors, are lower than 20%. Dusty days are more present during May – August (55% of NDD in sector I), April – August (56% of NDD at sector II), March – June (49% of NDD at sector III) and April – July (48% of NDD at sector IV). NDD at central and northern European sectors are more concentrated during late spring and early summer period. So, during the period May – June there are found 45% of NDD at sector V, 43% at sector VI and 39% at sector VII, while at sector VIII, 69% of NDD are found during a wider period; March – June. Almost the same distributions of the percentage data (even more concentrated at certain periods) are found also in the northern sectors. During May – June occur 60% of dusty days at sector IX, 74% at sector X and 66% at sector XI, while at sector XII, 81% of NDD are found during the period April – June. The annual cycles of NDD indicate that most of dust events over the whole continent occur during the late spring and early summer. Anyway, the evolution of NDD do not exactly follow that of the mean AOD, a result, previously obtained during the analysis in the sector I (Cachorro et al., 2016, Salvador et al., 2014).

3.3.2 Inter-annual trends of NDD in the European sectors

Analysis of the inter-annual variability of dust intrusions over European sectors was carried out based on the yearly averaged data of the number of dusty days, aerosol optical depth inside the dust plumes and percentage area covered by plumes, over each sector. No significant inter-annual trends were identified for NDD, AOD_p and PA during the 9-year period. Linear fit of the yearly-averaged data (in sector I) shows a slight decrease of NDD, AOD_p and PA, with R^2 0.22, 0.31 and 0.41, respectively. However, very low values of R^2 were obtained in the case of the other sectors, which don't let to assume any inter-annual trend. Also, previous studies confirm the absence of a significant inter-annual trend of AOD over the region. Pey et al., (2013) found no clear inter-annual trends of dust contribution on PM_{10} from 2001 to 2011.

The plots of the fig. 6 present the inter-annual variability of NDD, AOD_p and PA over twelve European sectors. The variability of the above-mentioned parameters is more evident in the southern sectors. A maximum of NDD was observed in 2010 in the sector III, and a minimum during 2011-2012 in the sector II. NDD in the other sectors show irregular variations (fig. 6.a). Fig. 6.b. show a gradual decrease of AOD_p only in the sector I, while the other sectors don't show any regular variation. PA follows almost the same variations as in the case of NDD (fig. 6.c.). This fact was supported also by the high CC between NDD and PA, 0.89.

To analyse the dispersion of the yearly NDD data for each sector; the coefficient of variation (CV) was used. Coefficient of variation is defined as the ratio of the standard deviation to the mean. This coefficient gives a measure of how dispersed a dataset is and can be used to compare distributions of different sizes and with different means (Erickson, and Nosanchuk, 1992). In terms of the coefficient of variation, the sector II has the lowest value (0.16), while CV was almost the same (0.47, 0.48 and 0.51) in the other three southern sectors. Thus, there are a more regular yearly number of dust events in the sector II. This may be also due to the higher NDD in this sector, compared to the other southern sectors. This statement is supported also by the NDD data at the central and northern sectors. CV at central sectors was (0.64-1.5), much higher than CV in the southern sectors. Even higher values of CV in the northern sectors are retrieved. CV in these sectors ranged between 2 and 3.

3.4 Scenarios of intense dust intrusions over the European sectors

3.4.1 Identification of the principal scenarios

Scenarios of intense dust intrusions over the complete European continent are analysed using a higher threshold; AOD_p>0.2. The higher threshold eliminates time-consuming analyses on the less intense dust intrusions and considers only most intense events, which more probably transport dust plumes northward the continent. 948 is the total number of the dusty days over the European continent over the period 1 January 2006 – 31 December 2014. 91.5% of them occur in the southern sectors, 8.1% in the central sectors, and only 4 cases occur in the northern sectors. Even a considerable number of dust events cover two or more sectors instantly, these numbers are taken into the analysis once. Ten scenarios are selected for detailed analyses over the European continent (fig. 7). Scenario A (includes dust intrusions through sector I), scenario B (through sector II), scenario C (through sector III), scenario D (sector IV), scenario E (sectors I and II), scenario F (sectors II and III), scenario G (III and IV), scenario H (sectors I, II and III), scenario K (sectors II, III and IV) and scenario L (other cases).

The principal characteristics of these scenarios of dust intrusions are presented in the table 4. These characteristics include the fraction of occurrences of each scenario, the number of sectors affected by every distinct dust event, according to each scenario, duration of dust events according to each scenario, the average value of AOD_p over their southern sectors for each scenario of dust intrusion. The number of the affected sectors, duration of dust events and the AOD_p, presented in table 4, describes the intensity of these intrusions and in this manner, are strongly correlated to each other. For this purpose, there are estimated the correlation coefficients among the mean values of NDD, fraction, no. sectors, duration and AOD_p (Table 4), according to different scenarios. High values of the correlation coefficient, CC, between them confirm this statement. CC among the scenario-averaged values of the number of the affected sectors, their duration and AOD_{max} are in the range 0.60 – 0.91. Negative correlations are obtained between the occurrences of dust events and the above-mentioned three other characteristics. Their low CC values, -0.14 – -0.65, do not indicate strong relationships. Negative values, in this case, indicate that the most intensive dust intrusions are less frequent than the less intensive dust intrusions.

The most frequent scenario of dust intrusion over southern Europe is the scenarios B (dust intrusions through the sector II), followed by scenarios E (dust intrusions through the sectors I and II) and A (dust intrusions through the sector I). 31.3% of the all dust intrusions follow the scenario B, whilst 18.8% and 14.2% belong to the scenarios E

and A. This result indicates that the southwestern Europe is by far, the most affected region by the desert dust intrusions. The fact that the Italian cluster is the most affected by dust intrusions, is in a very good agreement with findings from EARLINET Potenza and other Italian stations (Mona et al., 2014). Scenarios of dust intrusions are grouped again into three main groups; affecting one, two and three European southern sectors, during the same dust intrusion. 64.5% of all dust intrusions are one-sector intrusions, which means that dust intrusions, in this case, affect only one of the southern European sectors. Furthermore, 30.1% and 3.7% are respectively two and three-sector dust intrusions. This means that more frequent are those dust intrusions which affect few sectors. Only in 13 cases, dust intrusions affect three southern sectors simultaneously.

No clear longitude-gradient of the number of dust intrusions was observed for the scenarios A-D. Occurrences of dust intrusions over sector III display a clear minimum. However, clear latitude-gradients of the dust occurrences are obtained when grouped scenarios are considered. Higher occurrences of dust intrusions are found following the western scenarios. Among the two-sector group scenarios of dust intrusions, the western scenario E is 1.8 times more frequent than the central scenario F, while the last one is 12 times more frequent than the eastern scenario G. Moreover, among the three-sector group scenarios, the western scenario H is 1.6 times more frequent than the eastern scenario K.

One principal characteristic of dust intrusions is that the scenarios A-D (one-sector scenarios) have the lowermost AOD_p (0.24), the number of sectors affected (1.04) and the duration of dust intrusions (3.2). Higher values of these characteristics are found in the wide-scale dust intrusions, like two and three-sector scenarios; AOD_p (0.27-0.30), number of affected sectors (2.4-3.8) and duration of dust events (4.2-4.4).

Almost the same mean AOD_p and the number of affected sectors are observed for the eastern (D, G, and K) and western scenarios (A, E and H). However, the duration of the western scenarios (4.2) is much longer than that of the eastern scenarios (3.2).

3.4.2 Northward penetration of dust intrusions

The penetration of dust plumes toward northern regions would be expected to be more evident during the more intense dust intrusions. Data in table 5 shows the fractions of the dust intrusions over different sectors during each scenario which penetrate to the central and northern European sectors. There are found 84 cases of dust intrusions which affect also central sectors (V-VIII) and 4 cases which affect also the northern sector X. Central sectors VI and VII, are the most affected sectors by intense dust intrusions (37 and 20 cases, respectively), characterized by the threshold mean $AOD_p>0.2$. Among the central sectors, the sectors V-VI (western sectors) are affected in 55 cases, while the eastern sectors VII-VIII only in 29 cases. The unique northern sector (X) affected by intense dust intrusion is located on the west side of the northern sectors. This is another affirmation that the intense dust intrusions affect more the western part of the European continent than its eastern part.

Only 3.9% of all one-sector scenarios (15 cases) overpass the southern region and bring dust northerly. Scenario A affect more the sector V, while scenario B affects the sector VI. Also, 17.3% of the two-sector scenarios (38 cases) progress up to the central and northern sectors. The central sector VI is the most affected by the scenarios E and F.

However, three-sector scenarios (14 cases) show more ability to propagate the dust to the north. 42.8% of them bring dust plumes up to the central sectors.

Correlation coefficients between the mean AOD_p at the southern sectors and their respective values at the central sectors, I-V, II-VI, III-VII, and IV-VIII, were 0.58±0.05. The CC between the central sectors and their respective northern sectors were even lower. These values for the scenarios V-IX, VI-X, VII-XI, and VIII-XII were about 0.45±0.14. Even though these CC does not take very high values, these are enough to describe the patterns of dust intrusions over European sectors. Anomaly correlation is another tool for identifying the scenarios and the linkages between dust emissions at desert sectors and AOD increase in the European sectors. This parameter correlates points with maximal emission. Maps of anomaly correlations and the other maps not shown here, support the conclusions obtained using the correlation coefficients (Fig. 8). According to these maps, dust outbreaks from sector XIII progress toward western sectors I and V. Desert sector XIV affects more the sectors II and VI, but also the sectors III and IV. The eastern Saharan sector (XV) affects more the sectors III and VIII. The eastern sector IV is more affected by the Middle East deserts than the Arabian Desert.

3.5 Climatology of dust emission rates of desert sectors

3.5.1 Overall statistical considerations over dust emission in Saharan and Arabian Deserts

The first step in determining the contribution of the desert sectors over dust intrusions over distinct European regions is the determination of the climatology of the dust emission rates (EMI_DUST) at the four desert sectors. The mean dust emission rates at the four desert sectors are respectively; $9.2 \cdot 10^{-10} \pm 1.8 \cdot 10^{-10}$ (sector XIII), $12.1 \cdot 10^{-10} \pm 2.6 \cdot 10^{-10}$ (sector XIV), $6.0 \cdot 10^{-10} \pm 1.4 \cdot 10^{-10}$ (sector XIV) and $8.1.10^{-10} \pm 2.2 \cdot 10^{-10}$ (sector XVI) $kg \cdot m^{-2} \cdot s^{-1}$. Highest dust emission rates are encountered on the central Sahara, while the lowest on the eastern Sahara. No significant difference on overall average of EMI at the two deserts was found. Mean EMI at three Saharan Deserts was only 1.13 times higher than in the Arabian Desert. The major difference between the two deserts is the period when EMI reaches extreme values. Annual cycles of EMI, over four desert sectors, are shown in the fig. 9.

Maximums of monthly-averaged values of EMI were obtained during April (sector XIII), March – April (sector XIV), during March (sector XV) and during the period June – July (sector XVI). Saharan emission rates have almost similar annual cycles, while Arabian emission has a bimodal cycle; one during early spring, in February - March and another one during summer period June – July. Seasonal EMI maps (fig. 10) show the seasonal averaged values of emission rates during four seasons.

The highest EMI in desert areas is obtained during spring (EMI_{max} $5 \cdot 10^{-9}$ $kg \cdot m^{-2} \cdot s^{-1}$) and summer ($EMI_{max}$ $4 \cdot 10^{-9}$ $kg \cdot m^{-2} \cdot s^{-1}$) seasons. The most active desert region is the Chad depression (fig. 10). Other active regions are the deserts of the western Sahara, Arabia, and Libya. This result is in good agreement also with previous studies (Prospero et al., 2002; Washington et al., 2003). Inter-annual variations of the dust emission rates at the four desert sectors are displayed in fig. 11. Same as with the European sectors, no clear trend was identified at the four desert sectors during the 9-year period of analyses. At the Saharan sectors XIII and XIV, an increase of yearly-average EMI until 2008 was identified, followed then by a gradual decrease. In the sector XV, a maximum was reached

during the years 2009-2010. Meanwhile, the variation of EMI in the Arabian Desert shows a more complicated pattern.

3.5.2 Linkages of dust events over Europe with desert dust emissions

To identify the influence of each of the desert sectors at dust events at different European regions, the annual cycles of EMI (desert sectors XIII - XVI) and AOD (southern European sectors I - IV) have been analysed. Figure 12 shows the monthly variations of EMI at the desert sectors and AOD_p at the southern European sectors.

In general, figure 12 show similar annual cycles of the AOD_p in the southern European sectors with the cycles of EMI at the desert sectors. However, some discrepancies are observed. These patterns suggest that dust events at southern European sectors (I – III) are related to the dust emission processes in the respective Saharan sectors (XIII-XV). The maximums of AOD in sectors I – III, coincide with the maximums of EMI at sectors XIII–XV, but with one month postpone. The bimodal distribution of the EMI at Arabian sector XVI does not fit well with the one modal distribution of AOD at southeastern European sector IV. This implies no direct influence of the sector XVI on the dust events at the sector IV. The second maxima of EMI during June - July at the sector XVI do not affect sector IV with AOD maxima during April – May. This sector may be more affected by the dust activation at the sector XV, which reaches its maxima during February - April.

Additional information is taken from analysis of the correlation coefficients among the monthly-averaged data of AOD_p (sectors I-IV) and EMI (sectors XIII-XVI). In terms of CC, the western Saharan sector XIII, affect almost the entire southern European region. In this case, CC of EMI (XIII) with AOD_p (I-IV) is very high. It varies from 0.69 up to 0.84. Moreover, this sector affects more the central sectors II and III (0.79-0.84). The central Saharan sector affects more the sectors II-IV. High CC values are retrieved also in this case; 0.77-0.90, especially for the sectors II-IV (0.89-0.90). Also, the eastern Saharan sector, affects more the sectors II-IV (0.69-0.84), where the most affected is the sector III. Furthermore, the influence of the Arabic sector is moderate in terms of the correlation coefficients. CC varies from 0.11-0.53.

The maps of fig. 13 shows the distribution of the anomaly correlation during the months when southern European sectors reach their maximal AOD; sector I and II during June, sectors III and IV during April. It is obviously seen from the maps of the fig. 13 that the sector I is more affected by the sector XIII at its AOD maxima during June. During the same month, sector II reaches its AOD maxima, but no direct relationship to the sector XIV is observed. Sector II is likely affected by two or three desert sectors simultaneously. This is supported also by the highest AOD values obtained in the sector II compared to other sectors. Sector XV affects more the sector III during its AOD maxima in April. The Arabian Desert exerts no significant influence on the AOD at the sector IV. These findings agree well with previous studies, like Mona et al. (2006) and Papayannis et al. (2008).

3.5.3 Identification of potential sources during the most intensive dust events over European sectors

A higher threshold on AOD_p is used to categorize the most intensive dust events over the European sectors. There are identified several intensive dust events using threshold $AOD_p = 0.4$. In sectors, I, II, III, and VI are identified respectively 9, 25, 5 and 1 intensive dusty days. These data indicate that the sector II is the most affected sector also

by these intense events. The maximal value of AOD_p at its entrance into the southern Europe is an indication of the intensity of dust intrusions. Nonetheless, the duration of the dust events and numbers of sectors affected are good parameters to estimate the persistence of a dust event. The sectoral mean AOD_p over the sectors I, II, III and VI during the most intensive dust events were 0.44, 0.46, 0.45 and 0.40 respectively.

To estimate potential dust sources during the events over European sectors, cluster analysis of HYSPLT back-trajectories are performed. Typical dust transport from the desert clusters into European sectors is about 10 days. Thus, 120-hr back-trajectories are deemed to compute the cluster analyses during these dust events. HYSPLIT trajectories (frequency option) are performed for these sectors during the respective intensive dust events. The altitude of dust intrusions over the Mediterranean basin ranges between 3000 and 5000 m (Mona et al., 2006; Papayannis et al. 2008). Because of most of the dust is transported at this range of altitudes, cluster analyses are performed in this range of altitudes. Fig. 14 show only frequency trajectories only at some specific cases of intense dust events over the sectors I, II, III and VI. Dust intrusions over the sector I is transported only from the Saharan sectors XIII and XIV with 86% and 14% of all back-trajectories which originate at the Saharan sectors. Similar with the previous case, the sector II is affected by dust intrusions originating from the Saharan sectors XIII (75%) and XIV (25%). Almost 50% of all back-trajectories affecting the sectors III and VI originate from the sector XIII, while the sectors XIV and XV contribute each on around 25% of all back-trajectories. Arabian sector XVI contribute over the sectors I-VI is negligible during these intense dust events.

Even though the dust emission rates among the Saharan and Arabian Desert sectors do not differ too much, their contribution to the southern European sectors is quite different. Averaged percentile of the number of back-trajectories originated from the three Saharan sectors were 72%, 22%, and 5%, while the Arab sector contributes only about 1%, especially only to the southeastern European sector.

3.6 Case study; confirmation of the most intensive dust event using AERONET measurement data, MODIS data and HYSPLIT back-trajectories

The most intensive dust event over Europe, in terms of AOD_p, its duration and the number of the affected sectors, is the one, which occurred during May 2008. This dust event lasted for 30 days and affected all the European sectors; the southern and central European sectors (I-VIII), and one northern sector (X). However, not all the sectors are covered simultaneously during this dust event.

The dust intrusion entered in the European continent principally from the southern sectors I and II on 1st of May 2008. First peaks of AOD_p were observed in sector II (19 May), sector III (20 May) and the central sector VII (21 May). After that, a second intense dust intrusion was observed in sector I (26 May), sector II (27 May), sector IV (28 May), which progress to the central sectors V (27 May) and VI (28 May) and furthermore up to the northern sector X (29 May). Figure 15 shows the DREAM maps of the AOD550_DUST during most intense period of dust event; 19-28 May 2008. These eight maps, present major dust intrusion over the European content. The most intensive part of this dust event occurs during the last six days (Pappalardo et al., 2010).

Perturbations on the mean AOD_p were observed also in the central sectors. One day after the peak on the sector I, a lower peak was obtained in the sector V. The same discussion is valid also for the sectors II-VI and III-VII. From the two peaks on AOD_p at sector II, only the last one influences its northern sector VI. The sector VI reach its peak

one day after the second peak of the sector II. The northern sector X reaches also a peak of the mean AOD_p. This peak was obtained one day after the peak at the sector VI and two days after the peak at the sector II. Maximal values of the AOD_p during this dust intrusion were obtained in sector I (0.60) and the sector II (0.55). High values of the AOD_p, indicate an intense dust intrusion over the sectors I and II. The progression of the dust plume toward the northern sectors was carried out through the central and northern sectors V, VI and VII, up to the northern sector X.

In addition, measurement data provided by AERONET are used to verify the BSC-DREAM forecasts. Hourly mean data provided by the model are collocated in space and time with AERONET data, to evident their correlations. Specifically, for each point we calculate the differences between model and measurements. Table 6, presents the aerosol properties in specific AERONET sites during this dust event. AERONET measurements were averaged during the lowest solar zenith angles. There are compared hourly averaged values of measured CM_AOD_{500} (AERONET) with the correspondent hourly averaged forecasted AOD_{550} (BSC-DREAM) values, during 1-31 May 2008, over the selected sites. CM_AOD_{500} is chosen despite AOD_{500}, to exclude from the comparison the contribution on AOD of the fine particles. AERONET provided also data for the Angstrom Exponent (AE_{500}) and fine mode fraction (FMF_{500}). The AERONET data are retrieved in; IMAA_Potenza - Italy, Xanthi - Greece, Sevastopol - Russia, Munich University - Germany, Kanzelhohe Observatory – Austria and Venice - Italy. There are chosen AERONET sites with largest temporal coverage. High AOD_p and CM_AOD data and low AE data suggest the presence of dust events over-passing all the above stations. However, the high values of the AE_{500} and FMF_{500}, are encountered during this month in several sites.

The overall average of AOD_p provided by BSC_DREAM at all sites was 0.05 ± 0.10, while AERONET measurements give CM_AOD of 0.08 ± 0.11. Based on the nonparametric analysis (Wilcoxon test), at the 0.05 level, the difference of the population means is significantly different with the test difference (0). Thus, model data are generally lower than those provided by AERONET. The mean correlation coefficient between model and AERONET data at the six sites was significantly high, 0.80. The CC values in the table 6 are calculated using the hourly averaged data over each station. The high correlation between the BSC_DREAM and AERONET data is evident also from the plot presented in the fig. 17. Fig.17 presents the scatter-plot of hourly-averaged $CM\text{-}AOD_{500}$ provided by AERONET and AOD500_DUST forecasted by the model, in all sites. The CC between AOD500_DUST and CM_AOD found by Pérez et al. (2011) at two Iberian sites range was ~0.71. Basart et al. (2012) found low correlations (~0.35), of the AOD provided by the BSC-DREAM and AERONET. These discrepancies may be due to the AOD conversions by the model.

However, even lower correlations were found between AERONET data of $CM\text{-}AOD_{500}$ and the sectorial-averaged AOD500_DUST provided by the model. This fact suggests the difficulties of the sparse AERONET measurements on large domain assessments.

Moreover, satellite products, such as those provided by MODIS are used to verify the results obtained by the model. Aerosol Optical Depth taken from Aqua/MODIS over six AERONET sites are compared to the AOD550_DUST forecasted by the model. There are taken MODIS data when Aqua satellite overpass the six AERONET sites during the period 19-28 May 2008. This is the period with the most intense dust flux over Europe, which lets to better

comparison between model and satellite data. These data are compared with the point data of the model which coincide with the satellite overpassing times. The overall results of this comparison are presented in Table 6.
Mean values of AOD_{550} over these seven sectors, provided by BSC_DREAM and MODIS were 0.11±0.11 and 0.20±0.12 respectively, with a correlation coefficient 0.52. Higher AOD values provided by the satellite compared to those of the model are justified by the fact that MODIS measures the total AOD, while the BSC-DREAM forecasts only the dust contribution on AOD. In the sites where fine aerosols are present, like those with anthropogenic activities, the differences between satellite and model results. Thus, in Potenza, a site in the southern part of Europe (sector II) without much presence of anthropogenic activities and with strong presence of dust, there is observed the minor difference between model and satellite results, with mean difference 0.04. But, in central sites of Kazelhohe_Observatory and Sevastopol (sectors VI and VII), there are observed the highest difference between the mean values of model and satellite data, 0.13-0.14. Both these sites are characterized by strong presence of fine particles, where their contribution on AOD_{500} is 0.10-0.15 and Angstrom exponent is 1.24-1.37.

Comparison maps between MODIS and DREAM data are demonstrated in figure 16. AOD_{550} maps over sectors II and III are shown in this figure. The model reproduces the evolution of the northward dust plume, which originates from the Tunisia and northwest Libya, over the central and southern part of the Italian peninsula provided by MODIS images. The second maps of this figure don't show an exact reproduction of the dust plume evolution. BSC_DREAM forecasted that the plume overpasses the central and western part of Greece, while the MODIS images suggest that the main dust plume overpass the Aegean region. In the second case, the model forecasts the dust plume more westerly.
While the satellite AOD_{550} values reach up to 1.0 in several areas of both sectors, the model forecasted maximal values of dust AOD_{550} up to 3.0-3.5, with higher values in the sector II. The main problem of the satellite in large domain assessments is their spatial coverage. The absence of AOD data at distinct parts of the sectors influences in their average AOD. This influence depends on the spatial-temporal position of the dust plume.

4 Conclusions

The investigation of the climatology of dust intrusions over the European continent was performed using the database of Dust REgional Atmospheric Model, BSC- DREAM8b_v2.0. The AOD550_DUST and EMI_DUST are the principal aerosol parameters considered in the analysis. Analyses were carried out dividing the European continent into twelve sectors. Also, four desert sectors are considered.
The distribution of the AOD and number of dusty days over the twelve sectors is investigated. Southern sectors result more affected by dust events, where 81% of them occur in southern sectors. Anyway, there are encountered cases when the dust plume progress up to the northern sectors. During the late spring and early summer, there are identified the major number of dust events. The southwestern sector (Iberian Peninsula) makes an exception because it is affected by dust events later than other three southern sectors. Mean AOD_p was 0.155, 0.32 and 0.122, respectively in the southern, central and northern sectors. No clear inter-annual trend was observed in the AOD_p and for the number of the dusty days. Most of dust intrusions enter over the region of Italy (18.8%). In terms of

scenarios, one-sector scenarios, which are more frequent, rarely bring dust over central and northern sectors. Only dust intrusions which affect two or more south sectors can progress toward the central and northern sectors.

Regarding the dust emission rates over the desert sectors, the highest dust emission rates are encountered over the central Sahara, while the lowest one over the eastern Sahara. The highest EMI in desert areas is obtained during spring (5.10-9 kg.m-2s-1) and summer (4.10-9 kg.m-2s-1) seasons. The Saharan Desert is activated mostly in the spring while the Arabian Desert in the summer. No clear inter-annual trend was identified for the dust emission rates at the four desert sectors. Annual cycles of AOD at European sectors and EMI at desert sectors as well as the HYSPLIT back-trajectories indicate that the dust events over the western and central European sectors resulted related to the emission processes over the Saharan sectors. Also, eastern European sectors are affected by the eastern Saharan sector, while the Arab sector has a negligible effect. European central sectors are usually affected by more than one desert sector at a time.

As a case study, the most intensive dust event was taken into a more detailed analysis. This dust event lasted for 30 days and affected all European sectors, reaching up to its northern sectors. HYSPLIT back-trajectories, suggest that the western and central Saharan sectors are the principal contributors to this dust event. There are selected distinct AERONET sites over the European sectors and a comparison between aerosol measurement data provided by AERONET and dust AOD forecasted by the model was done. The model forecasted lower AOD, compared to the AERONET data, 0.05 and 0.08 respectively. However, high correlations between AERONET and BSC-DREAM point data were found, 0.80. In addition, MODIS products, such as AOD_{550}, were compared to the AOD500_DUST provided by the model. Also, MODIS provides higher AOD than the model, 0.18 and 0.08 respectively. The correlation coefficient between the mean values of AOD over these sites, provided by MODIS and DREAM was also high, 0.81.

Acknowledgments: Part of this research was supported by funds from the project Smart and Green Technologies for Innovative and Sustainable Societies in WB. We thank L. Mona and G. Pappalardo (CNR-IMAA Atmospheric Observatory, Potenza, Italy) for her comments and suggestions in preparing this paper. We would like to thank especially the Barcelona Supercomputing Center (BSC) for their continuous advices related to the model BSC-DREAM. The authors thank the NASA-MODIS staff and for making available data used here. We also thank all the PIs of the AERONET sites used in this study; H. Brent (Sevastopol), M. Wiegner (Munich_Univ.), G. Zibordi (Venice), D. Baumgartner (Kanzelhohe_Obs.), S. Rapsomanikis (Xanthi), for maintaining the sites and preparing data for this study. Some AERONET data used in this work were supported by the ACTRIS (Aerosols, Clouds, and Trace Gases Research Infrastructure Network) Research Infrastructure Project funded by the European Union's Horizon 2020 research and innovation programme under grant agreement n. 654169; by the Spanish Ministry of Economy and Competitivity (project TEC2015-63832-P) and EFRD (European Fund for Regional Development); by the Department of Economy and Knowledge of the Catalan autonomous government (grant 2014 SGR 583); by the Unidad de Excelencia Maria de Maeztu MDM-2016-0600 financed by the Agencia Estatal de Investigación, Spain.

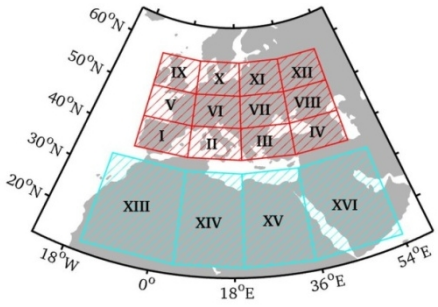

Figure 1: The affected European areas and the potential dust source areas. The European area is represented by twelve sectors (I-XII), while dust source areas contain three Saharan sectors (XIII-XV) and one Arabian sector (XVI).

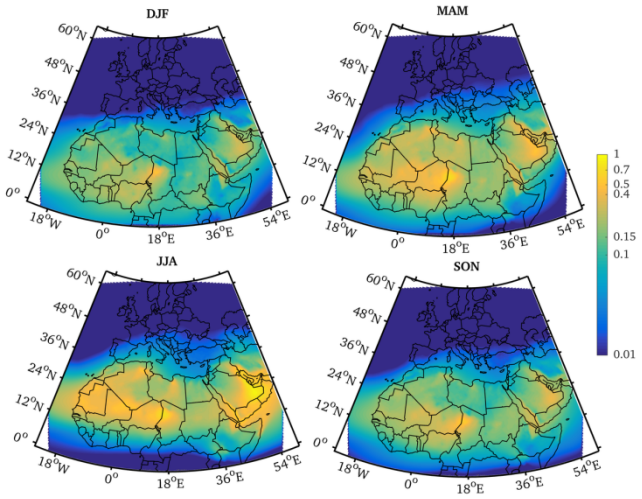

Figure 2: Maps of mean AOD550_DUST over Europe, and the nearby deserts of Sahara and Arabian Peninsula during four seasons; summer (JJA) and autumn (SON), winter (DJF) and spring (MAM). Mean AOD_{550} during the period 1 March 2006 – 30 November 2014, a period which includes the all consecutive seasons.

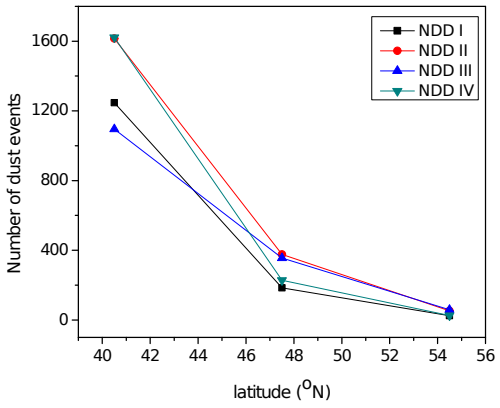

a)

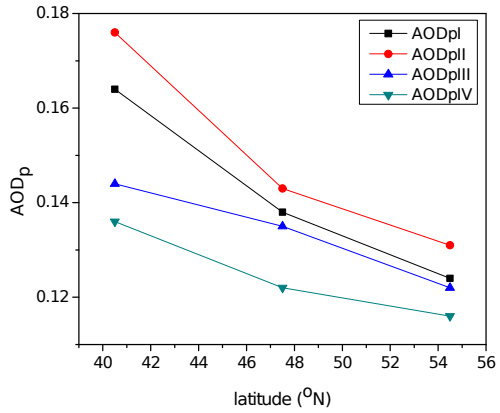

b)

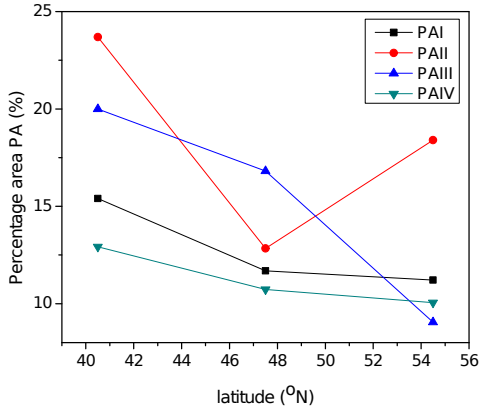

c)

Figure 3: The variations toward the latitude of a) number of dusty days (NDD), b) mean AOD_p of the dust plumes, and c) mean percentage area PA covered by dust plume, at each sector. The gradients are determined for the four southern European sectors, indexed by I, II, III and IV.

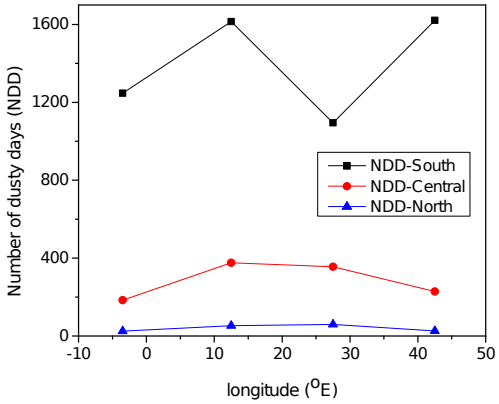

a)

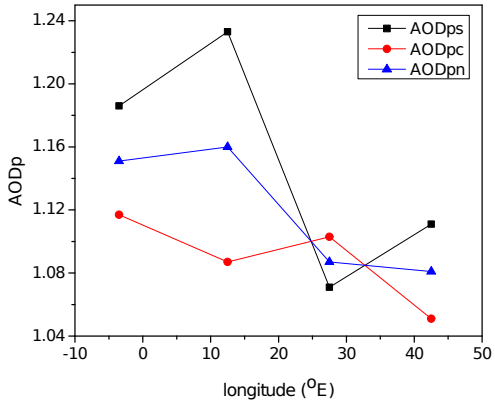

b)

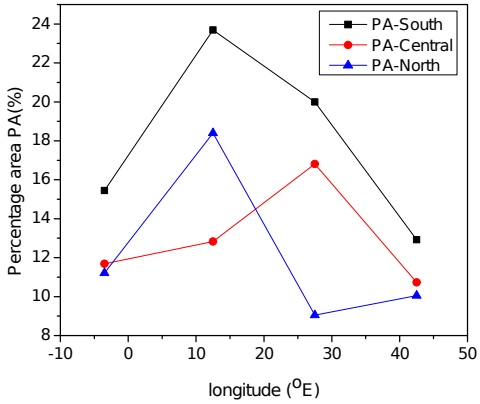

c)

Figure 4: The variations toward the longitude of a) number of the dusty days NDD, b) mean AOD_p of the dust plumes, and c) mean percentage area PA covered by dust plume, at each sector. The gradients are determined for the three European regions, indexed by S (south), C (central), and N (north). Here are presented the variations from the eastern to the central and from central to western sectors.

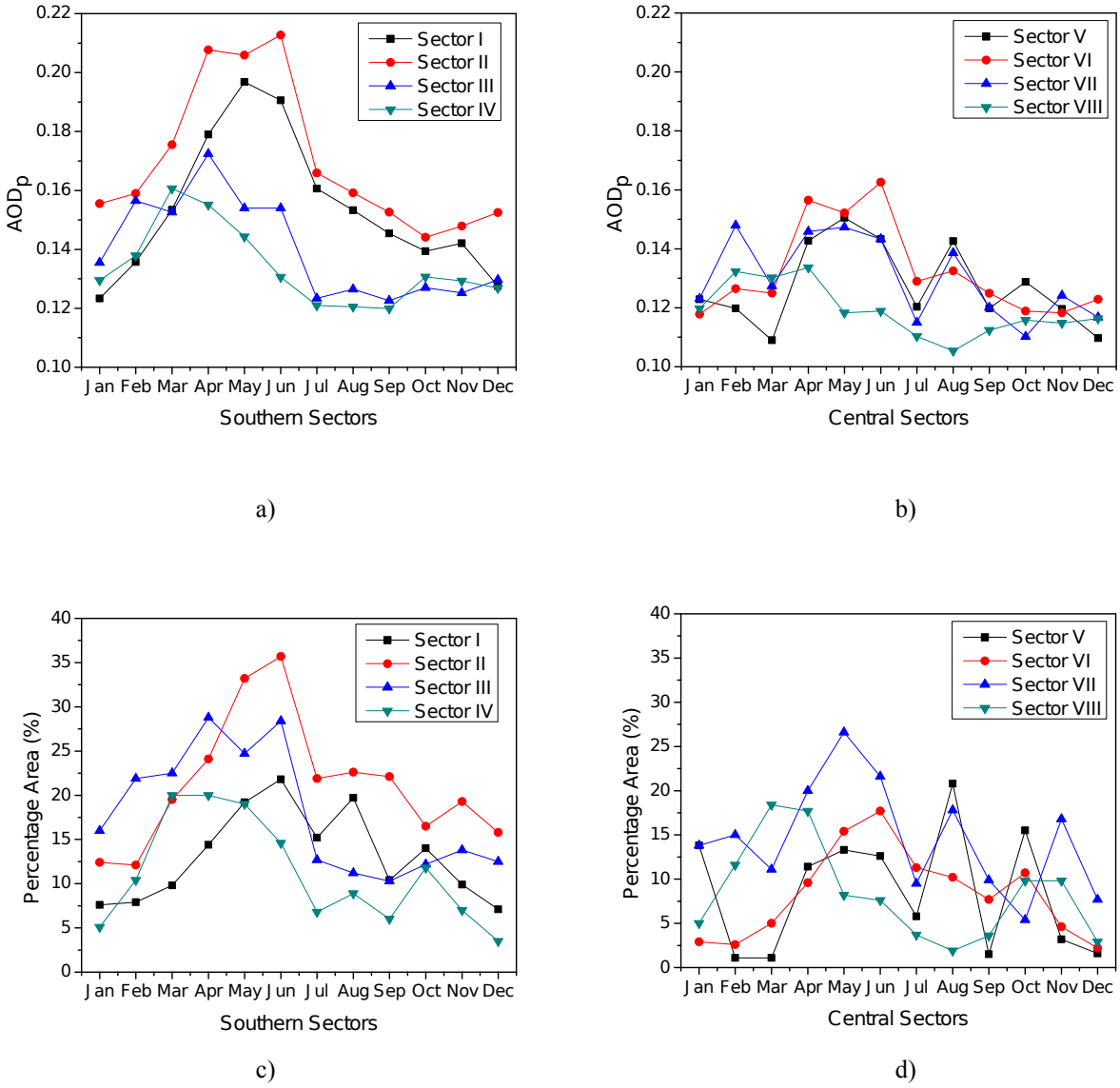

Figure 5: Annual cycles of Aerosol Optical Depth inside of dust plumes AOD_p, and the Percentage Area PA (%) at the southern and central European sectors (I-VIII).

a) AOD_p at southern sectors (I-IV), b) AOD_p at central sectors (V-VIII), c) PA at southern sectors (I-IV) and d) PA at central sectors (V-VIII).

.

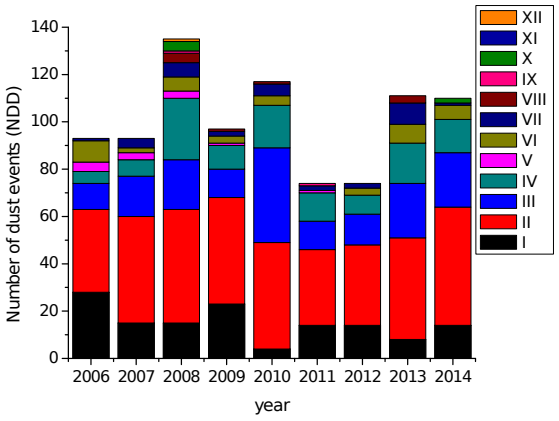

a)

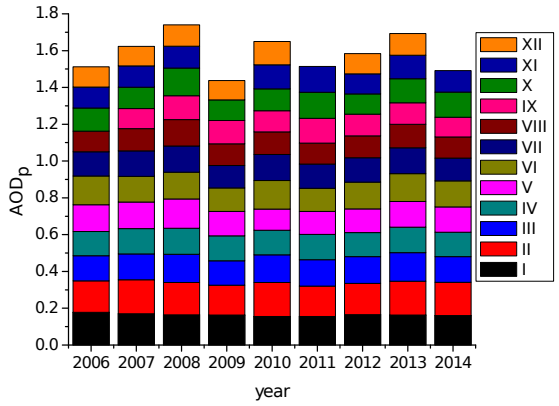

b)

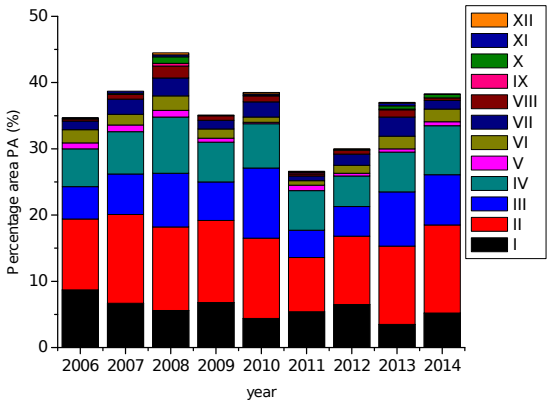

c)

Figure 6: The inter-annual variability of a) the number of dusty days NDD b) mean AOD_p of the dust plumes and c) mean percentage area PA covered by dust plume, at each sector, provided by the BSC-DREAM model, European sectors, for the 9-year period; 2006-2014.

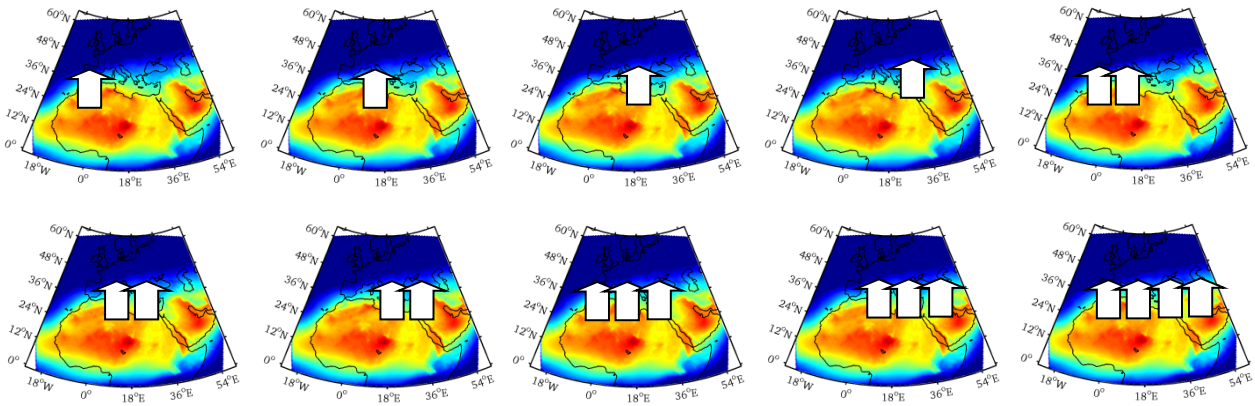

Figure 7: Ten principal scenarios of dust intrusions over southern European continent. First four scenarios (A-D) are only one-sector coverage, the next three scenarios (E-G) represent two-sector coverage intrusions, the next two scenarios (H-K) cover three sectors simultaneously while the scenario L represents the widt-range of dust intrusions.

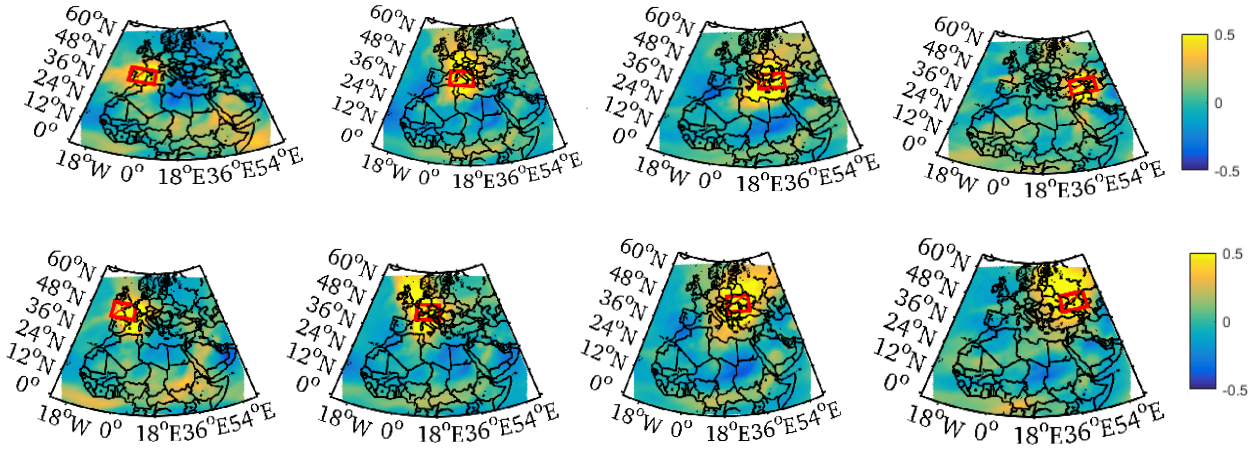

Figure 8: Anomaly correlations on the four southern European sectors (upper panel) and other four central sectors (lower panel). Anomaly correlations are calculated for each month, but here are shown only the maps in May, one of the most active month with dust events over Europe.

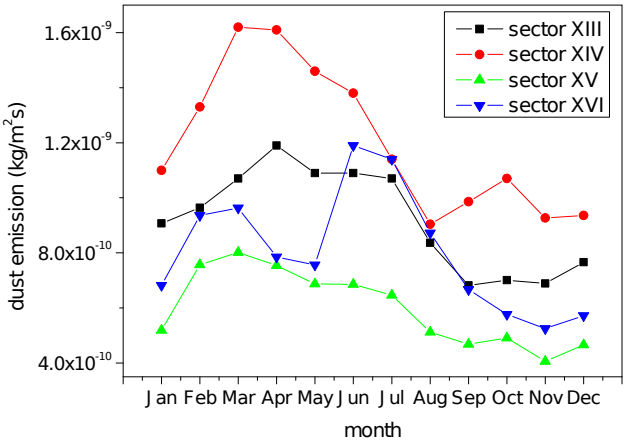

Figure 9: Annual cycles of dust emission rates (EMI) on four desert sectors; XIII (western Sahara), XIV (central Sahara), XV (eastern Sahara) and XVI (Arabian Desert).

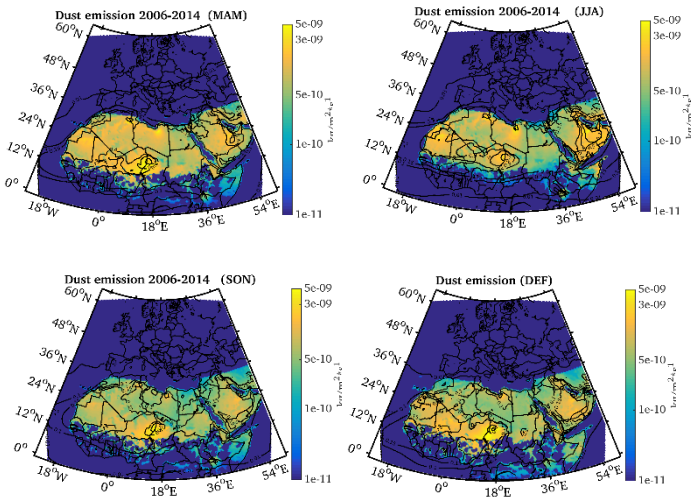

Figure 10: Dust emission rates EMI ($kg \cdot m^{-2} s^{-1}$) during four seasons; spring (MAM), summer (JJA), autumn (SON) and winter (DEF).

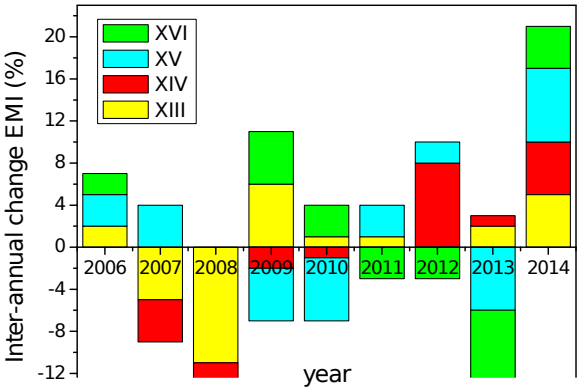

Figure 11: The inter-annual variability of the emission rates (EMI - % from the overall mean), provided by the BSC-DREAM model, at four desert sectors; three Saharan sectors (sectors XIII - XV) and Arabian Desert (sector XVI) for the 9-year period; 2006-2014.

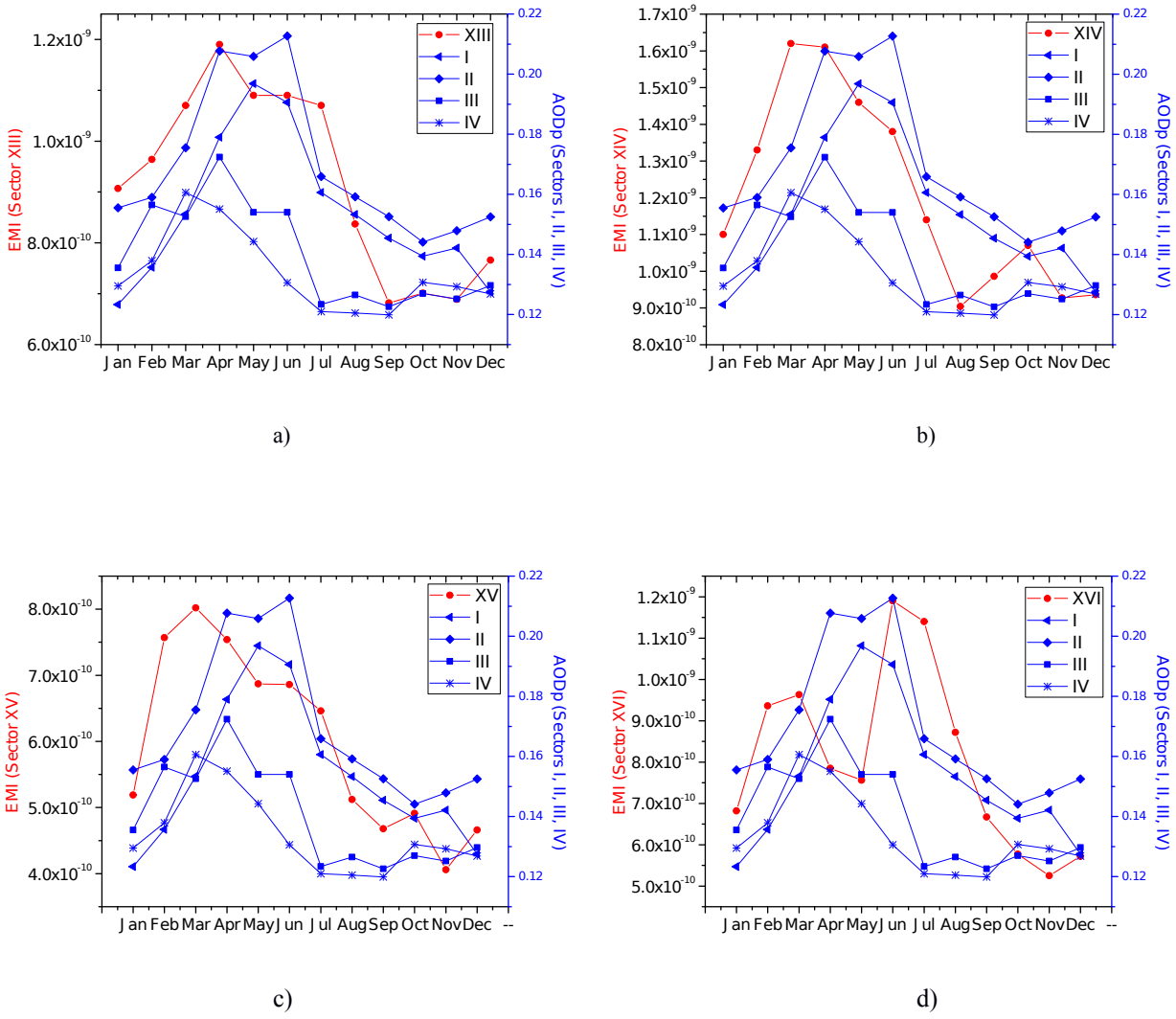

Figure 12: Comparisons of the annual cycles of AOD_p at the southern European sectors (I-IV) with those of EMI cycles in the desert sectors (XIII-XVI) are presented: a) desert sector XIII to southern sectors of Europe, b) desert sector XIV to southern sectors of Europe, c) desert sector XV to southern sectors of Europe, d) desert sector XVI to southern sectors of Europe.

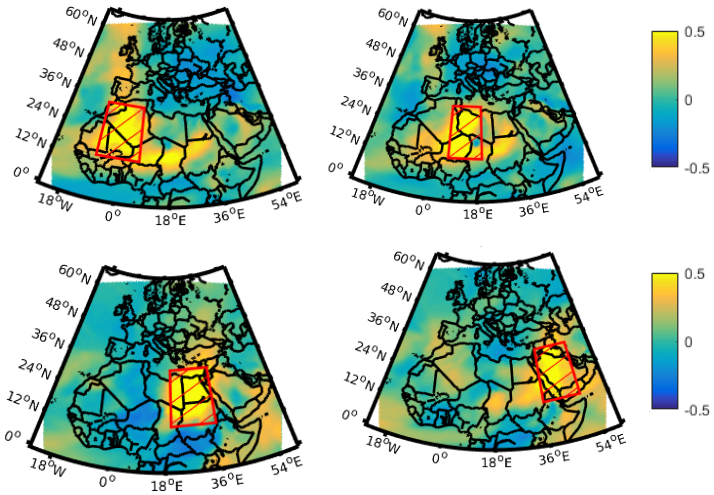

Figure 13: Maps of anomaly correlations during the months with maximal dust emission rates at the four desert sectors. Sectors XIII - XIV (during June), sectors XV - XVI (during April).

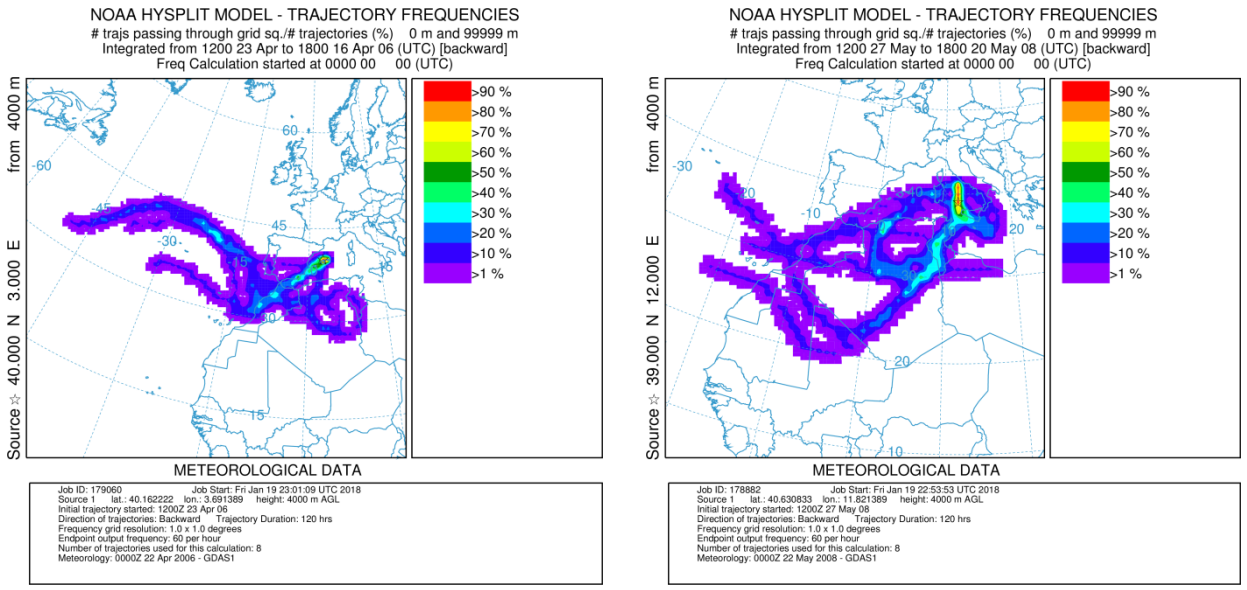

a) b)

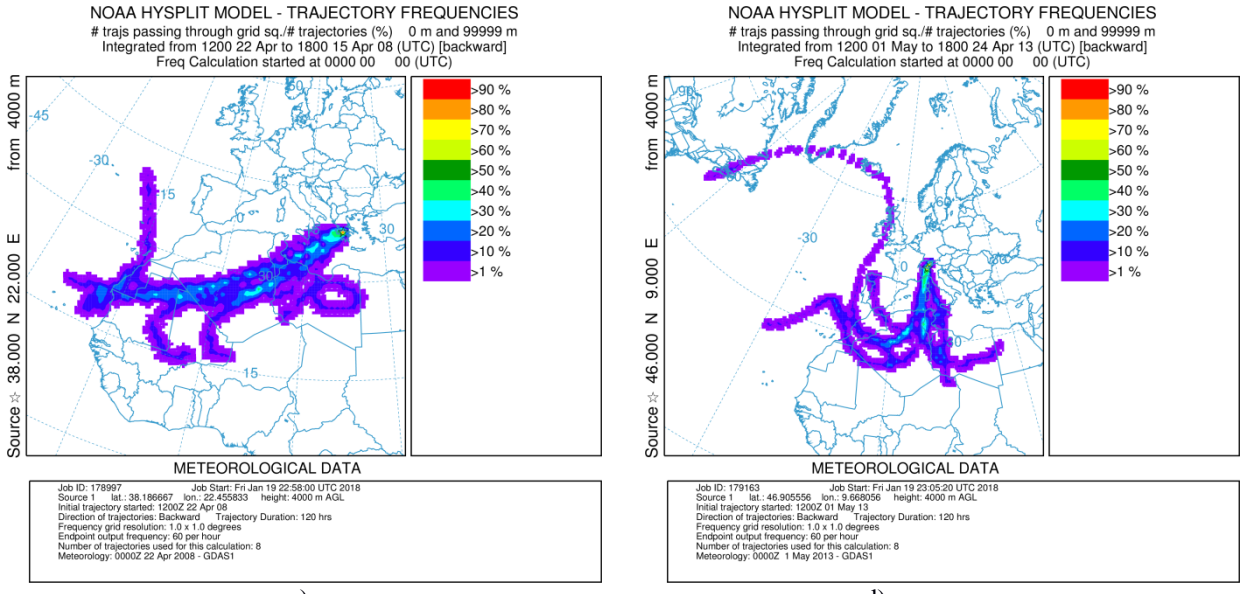

c) d)

Figure 14: HYSPLIT 120-hr frequency trajectories, performed at 4000 m a.g.l. during four distinct days of the intense dust event over the sectors; a) Sector I (23 Apr 06), b) Sector II (27 May 08), c) Sector III (22 Apr 08), and d) Sector VI (1 May 13). Not all the frequency trajectories are shown here.

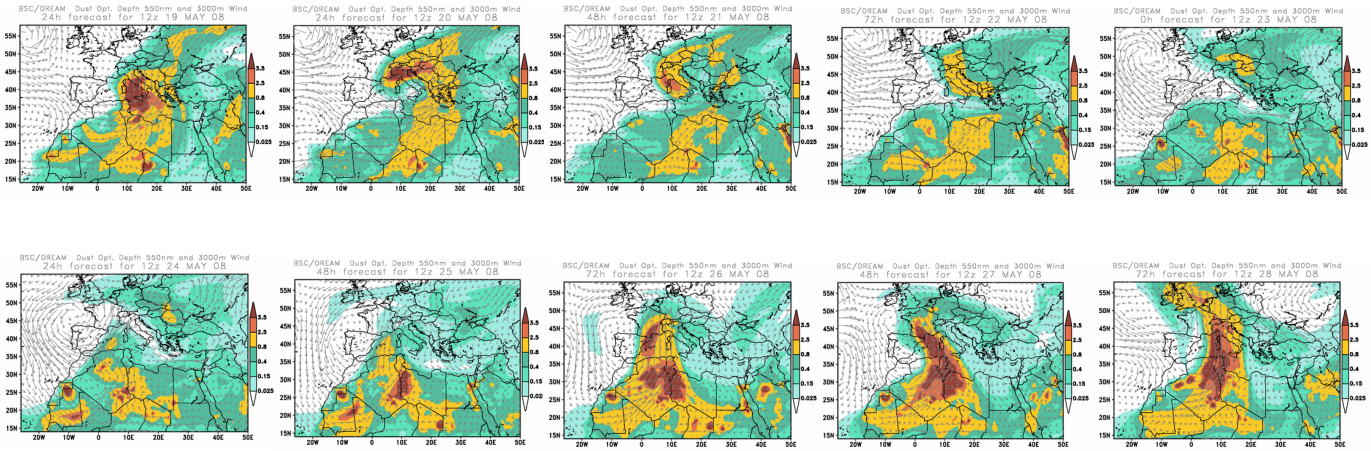

Figure 15: BSC-DREAM maps of AOD550_DUST, showing the progress of the dust plume toward the north of Europe. Here the most intense part of this dust event is presented; period 19-28 May 2008.

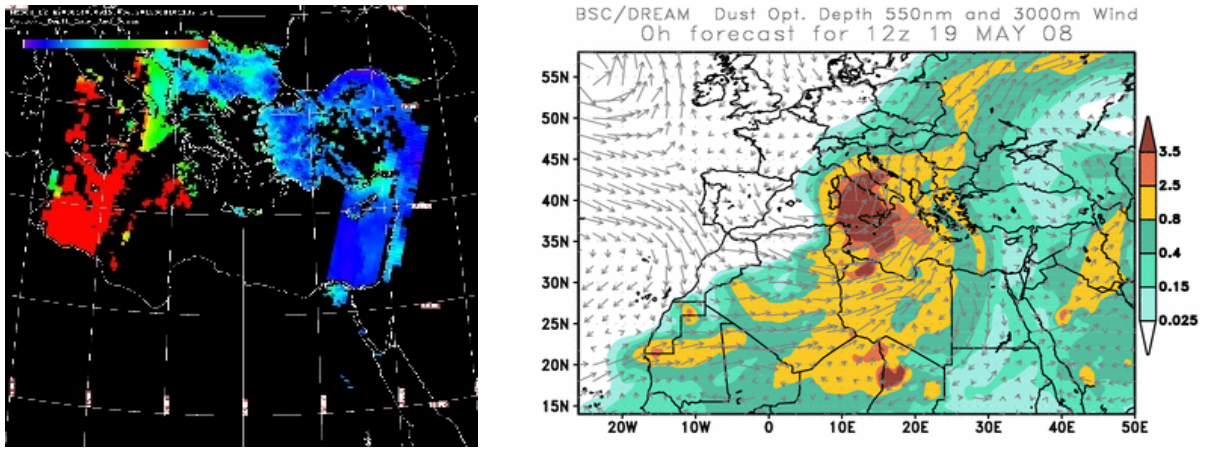

a)

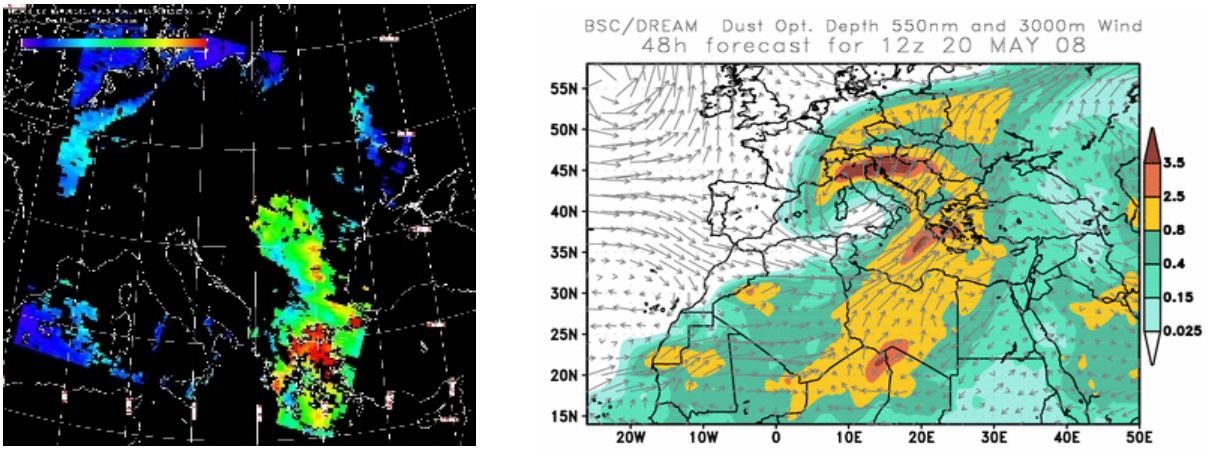

b)

Figure 16: MODIS and BSC-DREAM maps of AOD_{550} during 19-20 May 2008, when the sector II (upper figures) and the sector III (lower figures) reach their AOD peaks during the most intensive dust event.

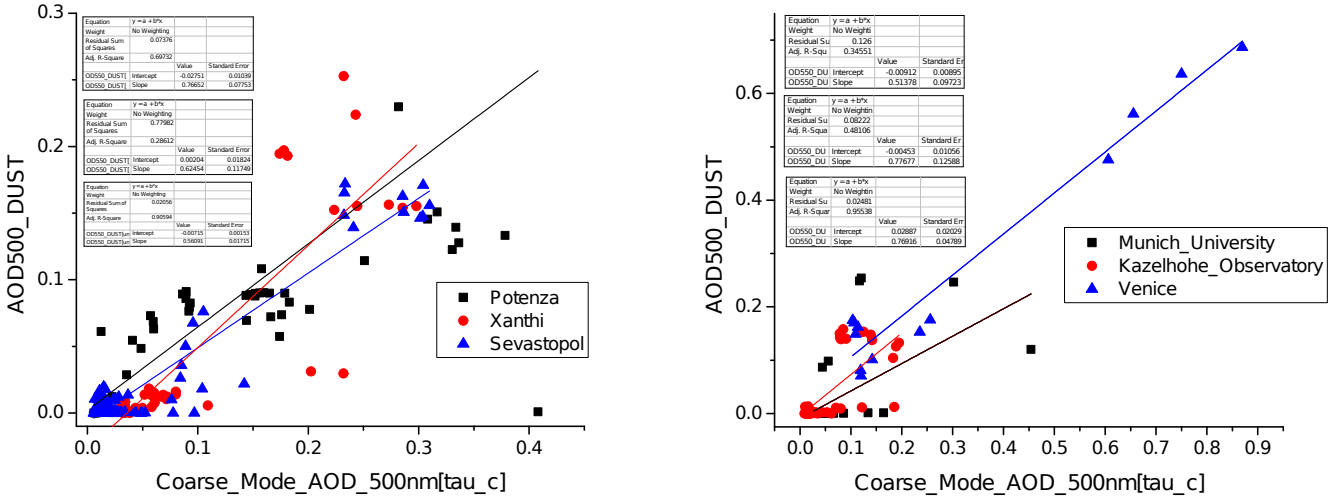

Figure 17. Scatter-plot of the AOD500_DUST data forecasted by the model and CM_AOD_{500} data measured in six AERONET sites. The data are divided into two groups for better presentation. Moreover, the linear fit of the plot data is presented.

Table 1: The mean AOD_p over the regions covered by the dust plume, the number of dusty days NDD, and the mean percentage area PA, for each sector are presented in this table. Mean data are associated with their standard deviation values.

Sec.	AOD_p	NDD	PA (%)
I	0.16±0.06	1247	15.4±18.0
II	0.18±0.07	1615	23.7±24.5
III	0.14±0.05	1095	20.0±23.7
IV	0.14±0.03	1621	12.9±16.3
V	0.14±0.04	184	11.7±15.2
VI	0.14±0.04	376	12.8±15.1
VII	0.13±0.04	356	16.8±18.0
VIII	0.12±0.02	228	10.7±15.4
IX	0.12±0.02	25	11.2±16.3
X	0.13±0.03	53	18.4±19.4
XI	0.12±0.02	59	9.0±9.5
XII	0.12±0.01	26	10.0±16.8

Table 2: Frequency distributions of mean AOD_p data (% of days) during dusty days at twelve European sectors. Five groups, based on the mean AOD_p values, are defined to estimate the distribution of the AOD data; $0.1<AOD_p<0.2$, $0.2<AOD_p<0.3$, $0.3<AOD_p<0.4$, $0.4<AOD_p<0.5$ and $0.5<AOD_p$.

AOD_p	**I**	**II**	**III**	**IV**	**V**	**VI**	**VII**	**VIII**	**IX**	**X**	**XI**	**XII**
0.1-0.2	80	74	90	94	92	90	94	97	100	92	100	100
0.2-0.3	16	19	8.9	5.5	7.6	8.2	5.1	2.6	0.0	7.5	0.0	0.0
0.3-0.4	3.5	5.4	0.9	0.2	0.5	1.3	0.8	0.0	0.0	0.0	0.0	0.0
0.4-0.5	0.6	1.3	0.5	0.0	0.0	0.3	0.0	0.0	0.0	0.0	0.0	0.0
>0.5	0.2	0.2	0.0	0.0	0.0	0.0	0.0	0.0	0.0	0.0	0.0	0.0

Table 3: The statistical distributions of the mean percentage area PA (%) data for each European sector. The two first rows present the coverage of 0.1% and 1% of each sector area. The other coverages are separated by 10%.

PA	I	II	III	IV	V	VI	VII	VIII	IX	X	XI	XII
0.1	2	1	3	2	3	2	1	4	4	6	0	0
1	14	9	17	17	21	15	12	21	20	11	14	23
10	53	41	51	61	67	59	51	69	72	45	64	73
20	21	16	15	18	14	20	17	14	12	19	24	12
30	10	13	9	9	5	9	12	6	4	11	10	8
40	6	8	6	6	5	6	8	6	4	11	0	4
50	4	6	6	3	4	4	4	2	0	2	2	0
60	3	5	4	2	4	1	3	1	8	6	0	0
70	2	3	4	1	1	2	2	1	0	2	0	0
80	1	3	2	0	0	0	2	0	0	4	0	0
90	1	3	2	0	0	0	1	0	0	0	0	4

Table 4: The principal characteristics of dust intrusions; the fraction occurrences of these events (%), number of sectors affected by the event, duration of the event (no. days) and the maximal value of AOD_{550} according to ten scenarios. Here, the above-mentioned characteristics are presented for every distinct scenario and their mean values for the grouped scenarios.

	According scenarios					**According grouped scenarios**		
	NDD	fraction	no sectors	duration	AODp	duration	no sec.	AODp
A	50	14.2	1.06	4.2	0.24	3.2	1.0	0.24
B	110	31.3	1.04	3.3	0.25			
C	28	8.0	1.03	2.9	0.24			
D	39	11.1	1.02	2.5	0.23			
E	66	18.8	2.22	4.7	0.27	4.2	2.4	0.27
F	37	10.5	2.30	4.2	0.29			
G	3	0.9	2.80	3.7	0.26			
H	8	2.3	3.56	4.8	0.29	4.4	3.8	0.30
K	5	1.4	4.00	4.0	0.30			
L	6	1.7	2.29	1.7	0.29			

Table 5: Fractions of dust events according to each scenario, which penetrate to the central sectors (sectors V-VIII) and northern sector X. Western and eastern sectors are grouped to better identify the influence of the different scenarios on western and eastern side of the continent. The percentiles of cases of the penetration of dust intrusions over central and northern sectors, as well as the percentiles of these intrusions which affect only the southern sectors, are presented.

	A	**B**	**C**	**D**	**E**	**F**	**G**	**H**	**K**	**L**
V	5/14	-	-	-	8/14	-	-	1/14	-	-
VI	1/37	6/37	-	-	16/37	9/37	-	3/37	1/37	1/37
VII	-	-	1/21	-	2/21	11/21	2/21	1/21	2/21	2/21
VIII	-	-	-	1/8	-	-	2/8	-	2/8	3/8
X	-	2/4	-	-	1/4	-	-	-	-	1/4
western	6/55	8/55	-	-	25/55	9/55	-	4/55	1/55	2/55
eastern	-	-	1/29	1/29	2/29	11/29	4/29	1/29	4/29	5/29
southern	94	96	97	98	81	70	20	44	0	0
central	6	4	3	2	19	30	80	56	100	100
northern	0	0	0	0	0	0	0	0	0	0

Table 6: AERONET data of aerosol optical depth (AOD_{500}), coarse mode contribution to AOD (CM_AOD_{500}), Angstrom exponent (AE_{500}), fine mode fraction FMF_{500} and BSC-DREAM data of AOD500_DUST over specific AERONET sites are presented. There are presented mean data during the period 1-31 May 2008, in Potenza-Italy, Xanthi-Greece, Sevastopol-Russia, Munich_University-Germany, Kanzelhohe_Observatory-Austria and Venice-Italy. Also, mean data of MODIS AOD_{550} and the correspondent BSC-DREAM AOD500_DUST, during the most intense period of this dust event, 19-28 May 2008, over these sites, are shown.

AERONET validation							**Satellite validation**		
AERONET				**DREAM**	**Diff.**	**CC**	**MODIS**	**DREAM**	**Diff.**
AOD_{500}	CM_AOD_{500}	FMF_{500}	AE_{500}	$AOD_{500}DUST$			AOD_{550}	$AOD_{500}DUST$	
Potenza									
0.22±0.12	0.11±0.11	0.56±0.28	0.94±0.52	0.07±0.13	0.04	0.54	0.10±0.06	0.07±0.06	0.04
Xanthi									
0.29±0.13	0.10±0.08	0.64±0.17	1.43±0.38	0.05±0.08	0.05	0.84	0.23±0.09	0.13±0.13	0.10
Sevastopol									
0.20±0.09	0.05±0.08	0.81±0.20	1.37±0.41	0.02±0.04	0.03	0.95	0.19±0.12	0.06±0.07	0.13
Munich_University									
0.16±0.06	0.06±0.07	0.72±0.12	1.54±0.24	0.02±0.06	0.04	0.60	0.10±0.06	0.01±0.01	0.09
Kanzelhohe_Observatory									
0.16±0.05	0.06±0.06	0.66±0.25	1.24±0.48	0.04±0.06	0.02	0.70	0.20±0.11	0.06±0.07	0.14
Venice									
0.46±0.36	0.32±0.29	0.35±0.08	0.71±0.36	0.28±0.22	0.05	0.98	0.26±0.20	0.16±0.16	0.10
Overall									
0.22±0.13	0.08±0.11	0.69±0.24	1.27±0.48	0.05±0.10	0.03	0.80	0.20±0.12	0.11±0.11	0.09